

# Self-supervised AutoFlow

Hsin-Ping Huang<sup>1,2</sup>, Charles Herrmann<sup>1</sup>, Junhwa Hur<sup>1</sup>, Erika Lu<sup>1</sup>,  
 Kyle Sargent<sup>1</sup>, Austin Stone<sup>1</sup>, Ming-Hsuan Yang<sup>1,2</sup>, Deqing Sun<sup>1</sup>  
<sup>1</sup>Google Research <sup>2</sup>University of California, Merced

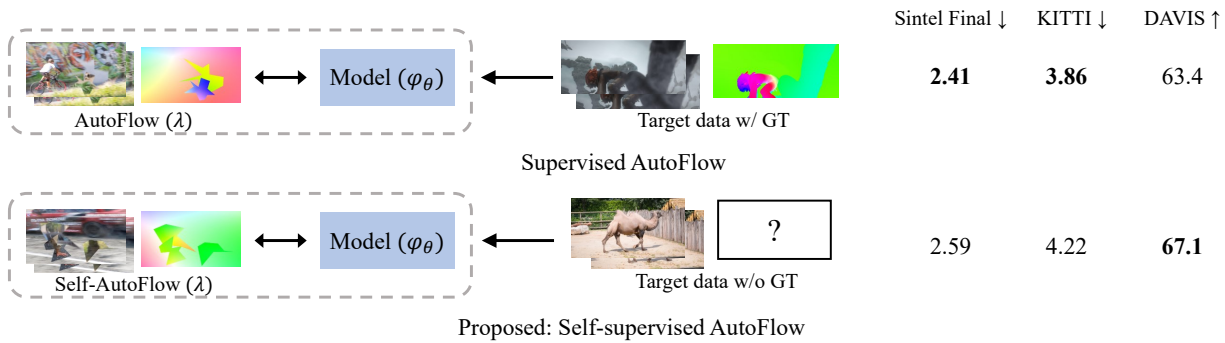


Figure 1. **Self-supervised AutoFlow** learns to generate a training set for optical flow using self-supervision on the target domain. It obtains similar performance as supervised AutoFlow on Sintel and KITTI despite not requiring ground truth (GT), and can learn a better dataset for the real-world DAVIS dataset, where GT is not available. We report optical flow accuracy on Sintel and KITTI, and keypoint propagation accuracy on DAVIS.

## Abstract

Recently, AutoFlow has shown promising results on learning a training set for optical flow, but requires ground truth labels in the target domain to compute its search metric. Observing a strong correlation between the ground truth search metric and self-supervised losses, we introduce self-supervised AutoFlow to handle real-world videos without ground truth labels. Using self-supervised loss as the search metric, our self-supervised AutoFlow performs on par with AutoFlow on Sintel and KITTI where ground truth is available, and performs better on the real-world DAVIS dataset. We further explore using self-supervised AutoFlow in the (semi-)supervised setting and obtain competitive results against the state of the art.

## 1. Introduction

*Data is the new oil.* — Clive Humby, 2006 [13]

This well-known analogy not only foretold the critical role of data for developing AI algorithms in the last decade but also revealed the importance of *data curation*. Like refined oil, data must be carefully curated to be useful for AI algorithms to succeed. For example, one key ingredient

for the success of AlexNet [21] is ImageNet [36], a large dataset created by extensive manual labeling.

The manual labeling process, however, is either not applicable or difficult to scale to many low-level vision tasks, such as optical flow. A common practice for optical flow is to pre-train models using large-scale synthetic datasets, *e.g.*, FlyingChairs [6] and FlyingThings3D [26], and then fine-tune them on limited in-domain datasets, *e.g.*, Sintel [4] or KITTI [28]. While this two-step process works better than directly training on the limited target datasets, there exists a domain gap between synthetic data and the target domain.

To narrow the domain gap, AutoFlow [41] learns to render a training dataset to optimize performance on a target dataset, obtaining superior results on Sintel and KITTI where the ground truth is available. As obtaining ground truth optical flow for most real-world data is still an open challenge, it is of great interest to remove this dependency on ground truth to apply AutoFlow to real-world videos.

In this paper, we introduce a way to remove this reliance by connecting learning to render with another independent line of research on optical flow, self-supervised learning (SSL). SSL methods for optical flow [15, 23–25, 54] use a set of self-supervised losses to train models using only image pairs in the target domain. We observe a strong correlation between these self-supervised losses and the ground

truth errors, as shown in Fig. 2. This motivates us to connect these two lines of research by adopting self-supervised losses as a search metric for AutoFlow [41], calling our approach “Self-supervised AutoFlow”.

Self-supervised AutoFlow obtains similar performance to AutoFlow on Sintel [4] and KITTI [28], where ground truth is available, and it can learn a better dataset for the real-world DAVIS data [29] where ground truth is not available. To further narrow the domain gap between synthetic data and the target domain, we also explore new ways to better synergize techniques from learning to render and self-supervised learning.

Numerous self-supervised methods, such as the recent SMURF method [38], rely on FlyingChairs [6] as a pre-training dataset. We can replace this pre-training stage with supervised training on AutoFlow data generated using self-supervised metrics and obtain improvements during the fine-tuning stages of SMURF.

This new pipeline is still self-supervised and obtains competitive performance among all methods that do not utilize the ground truth in the target domain. We further examine using self-supervised AutoFlow to obtain a strong initialization for supervised fine-tuning and obtain competitive results against the state of the art.

We make the following main contributions:

- We introduce self-supervised AutoFlow to learn a training set for optical flow using self-supervision on the target domain, connecting two independently studied directions for optical flow: learning to render and self-supervised learning.
- Self-supervised AutoFlow performs competitively against AutoFlow [41] that uses ground truth on Sintel and KITTI and better on DAVIS where ground truth is not available.
- We further analyze self-supervised AutoFlow in the semi-supervised and supervised settings and obtain competitive performance against the state of the art.

## 2. Related Work

**CNN architectures for optical flow.** Recent advances in deep learning and synthetic training datasets have resulted in numerous architectures for optical flow. Early work introduces basic architectures based on U-Net [6, 14, 35] or an image pyramid [32]. PWC-Net [42] introduces an advanced architecture design based on well-established domain knowledge (e.g. pyramidal processing, warping, and cost volume), together with a concurrent work, LiteFlowNet [12]. RAFT [43] proposes a more advanced architecture based on a full 4D cost volume with a recurrent optimizer, which significantly improves the accuracy of previous works and encourages numerous follow-up approaches [11, 18, 19, 39, 40, 45, 46, 53]. More recent work introduces attention-based architectures for optical flow [11, 17, 39, 46].

As our main focus is on the dataset, we adopt the widely-used RAFT architecture in our experiments.

**Self-supervised optical flow.** Supervised learning approaches may not generalize well to real-world domains where annotations are difficult to obtain. To overcome the limitation, self-supervised approaches [1, 33, 50, 54] directly train the networks on the target data with self-supervised losses, e.g., brightness constancy loss [15, 27], occlusion handling [44], knowledge distillation [23–25], *etc.* UFlow [20] systematically analyzes how each design choice from previous works affects the accuracy and introduces a combination that yields the best accuracy. SMURF [38] presents a self-supervised method using the RAFT [43] architecture and proposes several technical designs such as the sequence loss, full image warping, heavy augmentation, and multi-frame training. In this paper, we find that there is strong correlation between the self-supervised loss and the ground truth errors, which inspires us to use the self-supervised loss as a search metric to learn synthetic dataset. We further explore ways to synergize self-supervised methods and learning to render to improve performance in the unsupervised setting.

**Semi-supervised optical flow.** To benefit from both labeled (out-of-domain) data and directly training on target domains, semi-supervised approaches propose to reduce a domain gap between datasets [22] by using a GAN [7], to learn a conditional prior [49] from labeled data, to benefit from a small fraction of labels by active learning, [51] or to adapt to the target domain through knowledge distillation [16]. SemiFlow [9] introduces an iterative approach that generates a training dataset in the real-world domain using a pre-trained model and trains the model using the generated dataset. These methods usually rely on models trained on manually designed datasets, e.g., FlyingChairs and FlyingThings3D. Our work shows that using the self-supervised AutoFlow dataset can further improve the performance and, more importantly, remove manual design processes from the whole pipeline.

**Training datasets for optical flow.** Due to the difficulty of constructing large-scale real-world annotated datasets for optical flow, synthetic data (e.g. FlyingChairs [6], FlyingThings3D [26], Kubric [8]) have been widely utilized as standard (pre-)training datasets for optical flow. However, the datasets are generated without consideration of a target domain, so the domain gap always exists between the training and target domain, e.g., MPI Sintel [4], VIPER [34] and KITTI [28].

Two works have introduced a training dataset generation pipeline based on real-world images. Depthstillation [2] synthesizes an image at an arbitrarily rotated view from a still image and provides optical flow ground truth between the images. RealFlow [9] synthesizes an intermediate frame between two frames given an estimated flow. The synthe-

sis is controlled to have motion statistics similar to the target dataset. Both methods require off-the-shelf monocular depth methods [30, 31] and a hole-filling method to minimize artifacts on synthesized images. Furthermore, there is no guarantee that models trained on the synthesized datasets have optimal performance on the target domain.

AutoFlow [41] proposes a learning-to-render pipeline that learns dataset-rendering hyperparameters to optimize the optical flow accuracy on the target domain. Our method follows a similar direction, but unlike AutoFlow [41], our method does not require ground truth labels on the target domain; it uses a self-supervised search metric to update the rendering hyperparameters. It is therefore applicable to any target domain without available ground truth.

### 3. Approach

Given an unlabeled target dataset  $\mathbf{D}_{\text{target}}$ , we aim to learn a synthetic dataset  $\mathbf{D}_{\text{auto}}$  that approximately optimizes the performance in the target domain. To this end, we introduce self-supervised AutoFlow, which connects two independent research directions: (i) learning to render training datasets and (ii) self-supervised learning of optical flow (Sec. 3.2). Then, given the generated dataset  $\mathbf{D}_{\text{auto}}$  with ground truth and the unlabeled target dataset  $\mathbf{D}_{\text{target}}$ , our method trains an optical flow network  $\phi_\theta$  using self-supervision to further adapt to the target domain (Sec. 3.3). The whole pipeline is fully self-supervised and does not require any ground truth optical flow from the target domain.

#### 3.1. Preliminary: (Supervised) AutoFlow

AutoFlow [41] uses a layered approach to render a training dataset. The rendering pipeline uses a set of hyperparameters  $\lambda$  that control visual properties of foreground objects and the background (*e.g.* the number of moving objects, object shape, size, motion, *etc.*) and their visual effects (*e.g.* motion blur, fog, *etc.*) that appear in the rendered dataset. In a pre-defined hyperparameter search space  $\Lambda$ , an optimization process searches for an optimal set of hyperparameters  $\lambda^*$  such that an optical flow network  $\phi_\theta(\lambda)$  that is trained on a rendered dataset with the parameters  $\lambda$  minimizes a pre-defined search metric  $\Omega$  on the target dataset:

$$\lambda^* = \underset{\lambda \in \Lambda}{\operatorname{argmin}} \Omega(\phi_\theta(\lambda)). \quad (1)$$

AutoFlow [41] uses average end-point error (AEPE) for the search metric  $\Omega$  that measures the accuracy between available ground truth in the target dataset and estimated optical flow from the trained model  $\phi_\theta(\lambda)$ . Despite promising results on Sintel and KITTI, AutoFlow cannot be applied to real-world videos that do not have optical flow annotations.

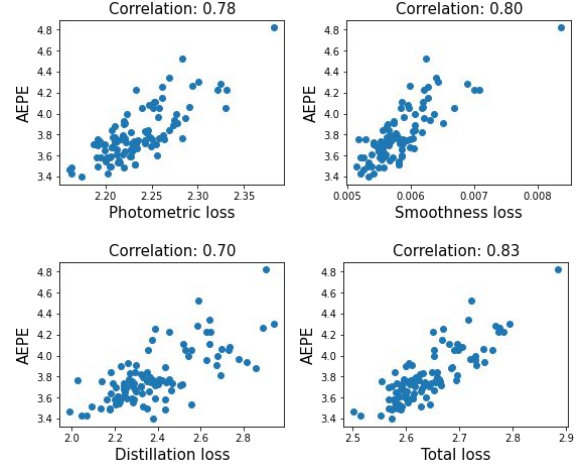


Figure 2. **Strong correlation** between ground truth error metric (AEPE) and self-supervised losses. We evaluate a set of RAFT models trained on supervised AutoFlow [41] datasets using the ground truth average end-point error (AEPE) and self-supervised losses averaged on the Sintel Final data. Each point in the plots indicates the performance of one model.

#### 3.2. Self-supervised AutoFlow

**Motivation.** To remove AutoFlow’s dependence on in-domain ground truth, we look for inspiration from another line of research: self-supervised learning for optical flow. In particular, the recent SMURF [38] outperforms the supervised PWC-Net [42] (the state of the art 4 years ago) on Sintel and KITTI, suggesting that its self-supervised loss is highly correlated with the ground truth errors and could be a good proxy metric for learning optical flow.

To this end, we analyze the correlation between the ground truth average end-point error (AEPE) metric and SMURF’s [38] self-supervised loss on Sintel using the trained models during the hyperparameter search of the supervised AutoFlow [41], as shown in Fig. 2. Each point in the plot corresponds to a RAFT model trained by a supervised AutoFlow dataset, with its AEPE on the Sintel Final split (*y* axis) and the self-supervised loss (*x* axis) that consists of a photometric loss, smoothness loss, and distillation loss. As shown in the plots, lower self-supervised losses correspond to lower AEPEs, and the correlation between the two signals increases when multiple losses are combined (*i.e.* total loss). This observation suggests that the self-supervised loss can also serve as a reliable proxy search metric and motivates our Self-supervised AutoFlow.

**Self-supervised search metric.** Our work extends the applicability of AutoFlow and presents Self-supervised AutoFlow (Self-AutoFlow or S-AF) which enables rendering a training dataset for a target domain by relying on the self-supervision loss metrics. We define our search metric  $\Omega$  using a self-supervised loss which consists of three terms,

a photometric loss  $\mathcal{L}_{\text{photo}}$ , a smoothness loss  $\mathcal{L}_{\text{smooth}}$ , and a distillation loss  $\mathcal{L}_{\text{distill}}$ ,

$$\Omega_{\text{S-AF}}(\phi_{\theta}(\lambda)) = \mathcal{L}_{\text{photo}} + \omega_{\text{smooth}}\mathcal{L}_{\text{smooth}} + \omega_{\text{distill}}\mathcal{L}_{\text{distill}}, \quad (2)$$

where each loss function follows that of SMURF’s [38] and  $\omega_*$  are weighting coefficients. The input to each loss term is a pair of input images and an estimated optical flow from a trained model  $\phi_{\theta}(\lambda)$ , and are omitted for brevity.

The photometric loss,  $\mathcal{L}_{\text{photo}}$ , penalizes the difference of corresponding pixels between input images  $\mathbf{I}_t$  and  $\mathbf{I}_{t+1}$ .  $\mathbf{I}_{t+1}$  is differentially warped into  $\mathbf{I}_t$  using the predicted optical flow,  $\mathbf{W}_t$ , and following [52], a Hamming distance of ternary-census-transformed image patches of corresponding pixels is used to compute the photometric loss with respect to  $\mathbf{W}_t$ . The smoothness loss,  $\mathcal{L}_{\text{smooth}}$ , uses the  $k^{\text{th}}$  order edge-aware smoothness to encourage continuity of the predicted optical flow field while allowing for discontinuity on image edges. The distillation loss,  $\mathcal{L}_{\text{distill}}$ , (*i.e.*, ‘self-supervision loss’ in SMURF [38]) applies a loss between a prediction on original images from a teacher model and a prediction on augmented and cropped images from a student model. As there is no backpropagation to the model in the search of AutoFlow, the search metric uses only the final, instead of all intermediate, flow prediction of RAFT.

**Mixed datasets.** Despite the high correlation between self-supervised loss and the ground truth error metric, there is no guarantee that the top candidate returned by self-supervised AutoFlow is the optimal set of hyperparameters according to the ground truth. To increase robustness, we choose the top-3 hyperparameter sets returned by self-supervised AutoFlow, generate a set of images with ground truth from each hyperparameter set, and mix them equally to form our final self-supervised AutoFlow dataset  $\mathbf{D}_{\text{auto}}$ . Empirically, we find that mixing the datasets decreases the likelihood of sampling a poor-performing AutoFlow hyperparameter and generally improves the robustness of the algorithm.

**Discussion.** There is a significant difference between (i) learning a training set using self-supervised search metrics and (ii) self-supervised learning for optical flow. The self-supervised optical flow methods are directly trained on a target dataset using self-supervised proxy losses. Gradients from the losses are directly backpropagated to update the model parameters. On the other hand, our self-supervised AutoFlow approach does not directly update the model using the self-supervised loss on the target domain. Instead, it optimizes hyperparameters for rendering a synthetic dataset. Our flow model is trained on the dataset generated by the hyperparameters. The high correlation between the self-supervised loss and the ground truth error makes the Self-AutoFlow dataset almost as good as the AutoFlow dataset. A different perspective is that the rendering pipeline serves as an inductive bias for self-supervised

learning and can model complex phenomena that are difficult to capture with the self-supervised loss, such as occlusions and motion blur.

### 3.3. Combining Self-supervised AutoFlow with Self-supervised Optical Flow

Given the AutoFlow dataset  $\mathbf{D}_{\text{auto}}$  learned from the self-supervised search metric, we further combine two data sources for training: (i) the self-supervised AutoFlow data  $\mathbf{D}_{\text{auto}}$  and (ii) a target dataset without ground truth  $\mathbf{D}_{\text{target}}$ . Specifically, we first pre-train the models on  $\mathbf{D}_{\text{auto}}$ , and then fine-tune the models on the target dataset  $\mathbf{D}_{\text{target}}$  based on a self-supervised training protocol, SMURF [38]. We briefly describe the fine-tuning approach below.

**Self-supervised fine-tuning.** We fine-tune the pre-trained model using the target dataset without labels (*i.e.* raw videos) to further adapt the model to the target domain. We use the same self-supervised loss from Eq. (2).

$$\mathcal{L} = \mathcal{L}_{\text{photo}} + \omega_{\text{smooth}}\mathcal{L}_{\text{smooth}} + \omega_{\text{distill}}\mathcal{L}_{\text{distill}}. \quad (3)$$

**Multi-frame fine-tuning.** After fine-tuning on the target domain with the self-supervised loss in Eq. (3), we further apply the multi-frame fine-tuning from SMURF [38]. Given a triplet of input frames ( $\mathbf{I}_{t-1}$ ,  $\mathbf{I}_t$ , and  $\mathbf{I}_{t+1}$ ), SMURF predicts bi-directional flow ( $(\mathbf{I}_t \rightarrow \mathbf{I}_{t-1})$  and  $(\mathbf{I}_t \rightarrow \mathbf{I}_{t+1})$ ) and generates pseudo ground truth for the forward flow  $\mathbf{W}_{\text{pseudo}}$  that includes more reliable estimation on occluded pixels through occlusion detection and inpainting using a shallow CNN. Then, we apply the following sequence loss from RAFT [43], which applies the  $l_1$  loss ( $\rho_F$ ) on each  $n^{\text{th}}$  intermediate output  $\mathbf{W}^n$  with a decay factor  $\gamma$ ,

$$\mathcal{L} = \sum_n \gamma^{N-n} \rho_F(\mathbf{W}_{\text{pseudo}} - \mathbf{W}^n). \quad (4)$$

## 4. Experiments

### 4.1. Experimental setup

We use RAFT [43] as the backbone architecture. For the self-supervised hyperparameter search, we train 16 models in parallel using 96 NVIDIA P100 GPUs. At each search iteration, we train models for a short amount of certain steps, evaluate them on our search metric (Eq. (2)), and update the hyperparameters. We conduct 8 search iterations, which results in  $16 \times 8$  total models for the search. We use the Adam optimizer ( $\beta_1=0.9$ ,  $\beta_2=0.999$ ) with a learning rate of 0.0001 and a one-cycle learning rate schedule [37].

For each target domain, we conduct a separate search and render a separate dataset. After pre-training a model on the rendered dataset, we further fine-tune the model with the self-supervised loss (Eq. (3)) on each target dataset. Then, we apply multi-frame fine-tuning using Eq. (4). We use a



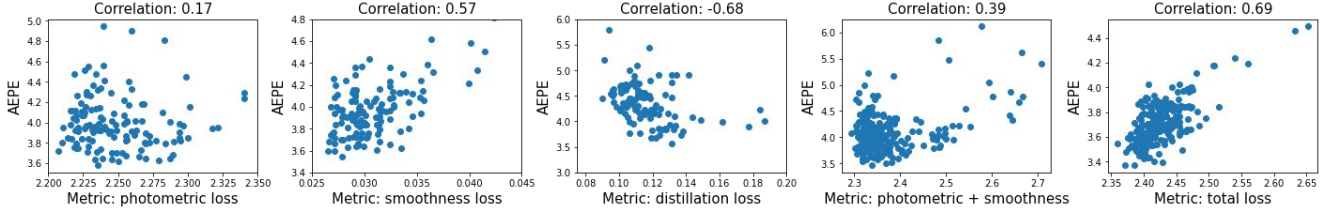


Figure 3. **Ablation study of self-supervised search metric.** None of the individual terms of the standard self-supervised loss function, when used as a search metric, is strongly correlated with AEPE. Only the combination of all three terms leads to a strong correlation between the search metric and the ground truth AEPE on the target dataset of a model trained on the generated dataset. Note that Fig. 2 shows the correlation of supervised AutoFlow models searched by ground truth error and Fig. 3 shows the self-supervised AutoFlow models searched by different self-supervised metrics.

Table 1. **Comparison of (self-)supervised pre-training approaches.** Our Self-AutoFlow (S-AF) outperforms FlyingChairs pre-training and is competitive with supervised AutoFlow (AF) which is learned from ground truth annotations. **Bold** indicates the best number. “AF X”, “AF-mix X” or “S-AF X” indicates that AF or S-AF is learned for the dataset X. Numbers in parentheses indicate the number of training steps.

Dataset and Method	Sintel Clean (AEPE ↓)	Sintel Final (AEPE ↓)	KITTI (AEPE ↓)
<b>Supervised</b>			
RAFT Chairs [43]	2.27	3.76	7.63
AF Sintel (3.2M) [40]	<b>1.74</b>	<b>2.41</b>	4.18
AF-mix Sintel (3.2M)	1.85	2.53	3.92
AF KITTI (0.8M) [41]	2.09	2.82	4.33
AF-mix KITTI (0.8M)	1.87	2.77	<b>3.86</b>
<b>Self-supervised</b>			
SMURF Chairs [38]	2.19	3.35	7.94
S-AF Sintel (3.2M)	<b>1.83</b>	<b>2.59</b>	5.22
S-AF KITTI (0.2M)	2.20	3.01	4.58
S-AF KITTI (0.8M)	1.99	3.00	4.29
S-AF KITTI (3.2M)	1.88	2.85	<b>4.22</b>

learning rate of 0.0002 with an exponential decay during the last 20% of steps. More implementation details are provided in the supplementary.

## 4.2. Self-supervised AutoFlow

**Comparison with the state-of-the-art pre-training approaches.** Tab. 1 compares our method with different pre-training approaches and reports the accuracy on Sintel and KITTI. All methods use RAFT [43] as the backbone architecture. AutoFlow (AF) [41] and our Self-AutoFlow (S-AF) is trained on each rendered dataset for Sintel or KITTI, and we report accuracy on both benchmark datasets. S-AF mixes rendered datasets from top-3 hyperparameter sets that show low metric score (see Sec. 3.2); for a fair comparison, we prepare an equivalent model for AutoFlow and denote it as AF-mix. “AF X”, “AF-mix X” or “S-AF X” indicates that AutoFlow (AF) or self-supervised AutoFlow (S-AF) is learned for the target domain X.

Our method substantially outperforms (self-)supervised pre-trained models on FlyingChairs and performs competi-

tive to the (supervised) AutoFlow and AutoFlow-mix. Note that supervised AutoFlow is guaranteed to outperform self-supervised AutoFlow. The small performance gap suggests that our self-supervised approach can successfully extend the applicability of AutoFlow on unlabeled target domains, which we demonstrate in Sec. 4.5.

**Ablation study of self-supervised search metric.** Fig. 3 provides an ablation study on our search metrics in Eq. (2). Similar to Fig. 2, each data point corresponds to a trained model with its AEPE on Sintel Final ( $y$  axis) and a loss value on a metric ( $x$  axis) that is used for our S-AF hyperparameter search. In Fig. 2, the hyperparameter search for AutoFlow is guided by a supervised signal (AEPE) and self-supervised signals (SMURF loss) are simply measured; in this setting, we observe a strong correlation between the model’s supervised performance and all individual self-supervised signals. This demonstrates that models on the search path of AEPE tend to have similar supervised and self-supervised performance. This does not prove that all models will share this property, nor does it prove that the models on the search path of a self-supervised signal will have this property.

In fact, when using self-supervision as a search metric, we observe very different behavior from Fig. 2. In practice, each of the individual self-supervised signals performs very poorly as a search metric. For example, a S-AF hyperparameter search guided by the distillation loss converges to models with very high AEPE but low distillation loss; to understand why, consider a model which predicts zero flow for any input. As a result, only the combination of all three self-supervised signals acts as an effective search metric; as shown in Fig. 3, the combination of all three losses results in models with the highest correlation between the search metric and the ground truth AEPE.

## 4.3. Self-supervised Learning of Optical Flow

**Comparison to the state of the art.** In Sec. 3.3, we combine our S-AF (Sec. 3.2) with the self-supervised learning approach of optical flow to further adapt the model to the

Table 2. **Comparison of self-supervised learning approaches.** Our models are pre-trained on self-supervised AutoFlow (S-AF) and the self-supervised objective (SS) using unlabeled data from the target dataset. Following SMURF [38], we train two models for each dataset on either the training split or the test split and evaluate on the other, denoted as **S-AF+SS train** and **S-AF+SS test**. Our method performs favorably against the state of the art. “{ }” trained on/using the unlabeled evaluation set; “[ ]” trained on data closed to evaluation set; “MF” using multi-frame estimation at test time [38].

Method	Sintel Clean [4]		Sintel Final [4]		KITTI 2015 [28]			
	AEPE ↓		AEPE ↓		AEPE ↓	AEPE (noc) ↓	F1-all (%) ↓	
	<i>train</i>	<i>test</i>	<i>train</i>	<i>test</i>	<i>train</i>	<i>train</i>	<i>train</i>	<i>test</i>
EPIFlow [54]	3.94	7.00	5.08	8.51	5.56	2.56	–	16.95
UFlow [20]	3.01	5.21	4.09	6.50	2.84	1.96	9.39	11.13
SemiFlow [16]	<b>1.30</b>	–	2.46	–	3.35	–	11.12	–
SMURF test [38]	1.99	–	2.80	–	2.01	1.42	6.72	–
S-AF+SS test	1.65	–	<b>2.40</b>	–	<b>1.94</b>	<b>1.37</b>	<b>6.56</b>	–
DDFlow [24]	{2.92}	6.18	{3.98}	7.40	[5.72]	[2.73]	–	14.29
SelFlow [25] <sup>(MF)</sup>	[2.88]	[6.56]	{3.87}	{6.57}	[4.84]	[2.40]	–	14.19
UnsupSimFlow [15]	{2.86}	5.92	{3.57}	6.92	[5.19]	–	–	[13.38]
ARFlow [23] <sup>(MF)</sup>	{2.73}	{4.49}	{3.69}	{5.67}	[2.85]	–	–	[11.79]
RealFlow [9]	{1.34}	–	{2.38}	–	{2.16}	–	–	–
SMURF train [38]	{1.71}	3.15	{2.58}	4.18	{2.00}	{1.41}	{6.42}	6.83
S-AF+SS train	{1.51}	<b>3.03</b>	{2.30}	<b>3.98</b>	{1.96}	{1.38}	{6.26}	<b>6.76</b>

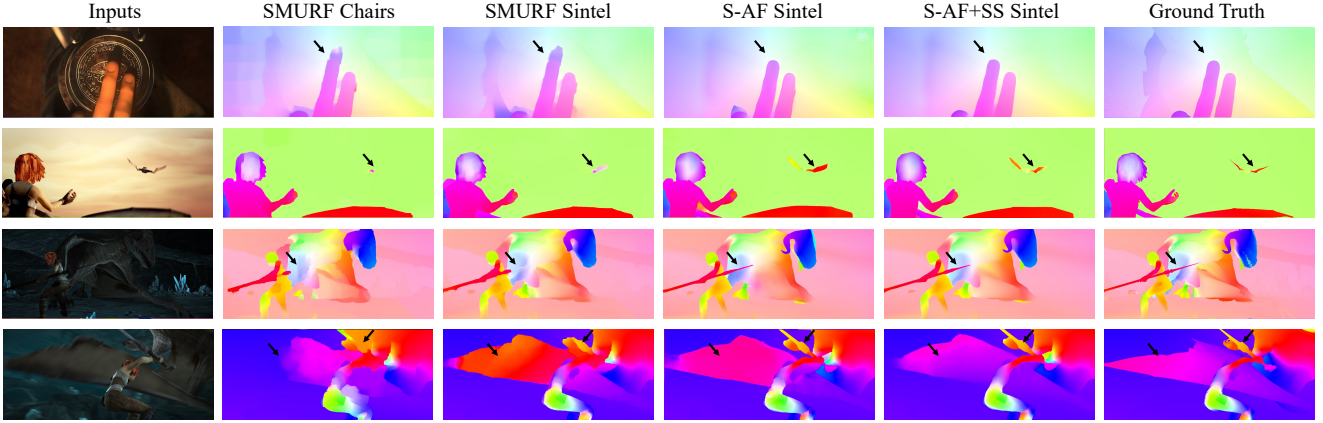


Figure 4. **Comparison of self-supervised methods on Sintel.** SMURF, both pre-trained (SMURF Chairs) and self-supervised fine-tuned (SMURF Sintel), tends to fail on shadows, strong motion blur, or small/thin objects. On the other hand, self-supervised AutoFlow (S-AF) on Sintel provides more reliable predictions, and self-supervised (SS) fine-tuning (S-AF+SS Sintel) further improves the results.

target domains, denoted by **S-AF+SS**.

We compare against state-of-the-art approaches that do not use ground truth in the target domain in Tab. 2. We train our model on the standard train/test splits for Sintel, and we train on the multi-view extension data following [38] for the KITTI dataset. We train two models for each dataset, one trained on the test split (\* test) in a self-supervised manner and evaluated on the training split with ground truth, and the other trained on the training split (\* train) and evaluated on the test split (*i.e.*, benchmark websites).

Compared to SMURF, our method reduces the AEPE by 0.13 on Sintel Clean test, 0.21 on Sintel Final test, and F1-all by 0.07 on KITTI test. Our method is comparable to SemiFlow and RealFlow on Sintel Clean train, although both SemiFlow and RealFlow are pre-trained on

FlyingChairs and FlyingThings3D and thus have strong performance on Sintel Clean, due to the proximity of their domains. Our method outperforms SemiFlow and RealFlow on the more challenging Sintel Final train and KITTI.

**Generalization across datasets.** In Tab. 3, we evaluate the generalization of our approach by training the model on one dataset and evaluating it on other datasets. We denote the models with self-supervised fine-tuning on target datasets as +SS Sintel/KITTI. When only training on S-AF datasets, RAFT achieves an AEPE of 1.83 on Sintel Clean and 2.57 on Sintel Final, which outperforms SMURF’s results with self-supervised fine-tuning on the target Sintel dataset by 0.16 and 0.23. Both RAFT trained on S-AF and self-supervised fine-tuned on Sintel/KITTI achieve the best cross-domain performance on all the tar-

Table 3. **Generalization across datasets.** We compare the generalization ability of self-supervised optical flow methods. We train the models on one dataset and evaluate on others. Our method (S-AF) outperforms SMURF on cross-dataset evaluations. SS Sintel/KITTI means further self-supervised training on Sintel/KITTI.

Method	Chairs	Sintel <i>train</i>		KITTI-15 <i>train</i>	
	<i>test</i>	Clean	Final	AEPE	Fl-all (%)
SMURF Chairs	1.72	2.19	3.35	7.94	26.51
S-AF Sintel	<b>1.61</b>	<b>1.83</b>	<b>2.57</b>	4.79	15.47
S-AF KITTI	2.09	2.16	2.96	<b>4.28</b>	<b>13.60</b>
+ SS Sintel					
SMURF	1.99	1.99	2.80	4.47	12.55
S-AF	<b>1.81</b>	<b>1.65</b>	<b>2.40</b>	<b>4.28</b>	<b>12.45</b>
+ SS KITTI					
SMURF	3.26	3.38	4.47	2.01	6.72
S-AF	<b>3.19</b>	<b>3.32</b>	<b>4.44</b>	<b>1.94</b>	<b>6.56</b>

Table 4. **Supervised fine-tuning on public benchmarks.** We fine-tune our model using ground truth in a supervised manner. (AEPE ↓ for Sintel and Fl-all ↓ for KITTI. Methods using warm start on Sintel are marked by \*). Models pre-trained on self-supervised AutoFlow (S-AF) can serve as a good initialization for supervised fine-tuning. Numbers in the parentheses indicate the number of training steps.

Method	Sintel Clean	Sintel Final	KITTI
RealFlow [9]	-	-	4.63 %
SemiFlow (RAFT)* [16]	1.65	<b>2.79</b>	4.85 %
RAFT-it (1.2M) [40]	1.55	2.90	4.31 %
RAFT-S-AF (0.6M)	<b>1.42</b>	2.99	<b>4.12 %</b>

get datasets.

#### 4.4. Supervised Fine-tuning on Public Benchmarks

To examine how well our method can serve as a good initialization, we fine-tune our S-AF+SS train model in Tab. 2 model using the same fine-tuning protocol from [40]. As shown in Tab. 4, our method is slightly worse on Sintel Final but more accurate on Sintel Clean and KITTI than RAFT-it [40], despite using half of the fine-tuning steps. It is more accurate than SemiFlow and RealFlow on KITTI, indicating that S-AF+SS models can serve as a good initialization for supervised fine-tuning.

#### 4.5. Keypoint Propagation on BADJA

To further demonstrate the generalization of our method to a real-world domain without ground truth, we compare our method with various supervised, semi-supervised, and self-supervised methods on the DAVIS dataset [29]. For the self-supervised fine-tuning on DAVIS, we use the seven BADJA sequences and three challenging sequences (drift-turn, drift-chicane and color-run) as the test set, and use the remaining 80 sequences for training. For evaluation, we use the Percentage of Correct Keypoint-Transfer (PCK-T) metric [48] with keypoint annotations from the BADJA dataset [3]. Given annotated keypoints on a reference im-

Table 5. **Keypoint propagation on the BADJA dataset [3].** We use different optical flow methods to generate the trajectory of keypoints in sequences and report the PCK-T metric. The optical flow is predicted from the adjacent frames and used to propagate the keypoints along the whole sequence. (S-)AF: (self-supervised) AutoFlow; SS: self-supervised fine-tuning. SMURF DAVIS is first trained on Chairs and then fine-tuned on DAVIS.

Method	bear	camel	cows	dog	horse-h	horse-l	Avg.
DINO [5]	83.3	58.6	71.2	68.9	46.7	57.5	64.4
PIPs [10]	81.5	83.8	79.8	68.3	78.9	61.3	<b>75.6</b>
<b>(Semi-)supervised</b>							
SemiFlow-DAVIS [16]	74.7	73.6	72.0	62.1	45.7	35.9	60.7
RealFlow-DAVIS [9]	79.6	73.6	72.3	63.1	52.4	28.7	61.6
AF Sintel [41]	81.2	77.6	73.9	72.8	46.7	28.1	63.4
RAFT-it [40]	82.4	83.7	78.8	70.9	46.7	34.1	<b>66.1</b>
<b>Pre-training</b>							
SMURF Chairs [38]	89.4	74.6	74.5	66.0	46.7	33.5	64.1
S-AF Sintel	82.0	85.1	62.8	65.0	50.5	30.5	62.7
S-AF KITTI	81.2	77.6	74.5	70.9	44.8	36.5	64.2
S-AF DAVIS	82.0	78.0	76.4	72.8	53.3	40.1	<b>67.1</b>
<b>Self-supervised fine-tuning</b>							
SMURF DAVIS [38]	89.8	84.1	79.6	75.7	58.1	44.9	72.0
S-AF+SS DAVIS	89.8	83.4	75.5	78.6	57.1	47.9	<b>72.1</b>

age, the metric calculates the percentage of correctly propagated keypoints along a video sequence. For a reliable optical flow evaluation, we discard the *dog-agility* sequence which presents heavy occlusion [47] between frames. We also exclude all keypoints once they become occluded according to the annotations since the keypoint propagation is no longer valid for optical-flow-based methods.

Tab. 5 shows that our S-AF DAVIS model achieves better accuracy than other supervised/semi-supervised approaches (SemiFlow, RealFlow, AF Sintel, RAFT-it) and a self-supervised pre-training (SMURF Chairs).

Our self-supervised fine-tuned model on DAVIS (S-AF+SS DAVIS) performs slightly better than SMURF DAVIS. Compared to the S-AF results that use different unlabeled data as target, S-AF DAVIS outperforms S-AF Sintel and KITTI, showing that our learning-to-render method successfully learns a better dataset for the target domains without using the ground truth labels. Compared with the long-term tracking method PIPs, S-AF DAVIS performs worse on horse sequences with fast motion, but on par or better on the other sequences, suggesting that these two methods may be complementary to each other.

#### 4.6. Visual Comparison

**Sintel.** As in Fig. 4, compared to out-of-domain pre-training approaches, S-AF Sintel performs better than SMURF Chairs on shadows, small/thin objects and scenes with strong motion blur. Self-supervised fine-tuning on Sintel (S-AF+SS Sintel model) further improves the results upon the pre-training S-AF Sintel model, whereas SMURF still tends to fail on those cases. The results show that our self-supervised learning-to-render approach not only provides a strong pre-trained model on the target domain, but also serves as a good initialization for the self-supervised

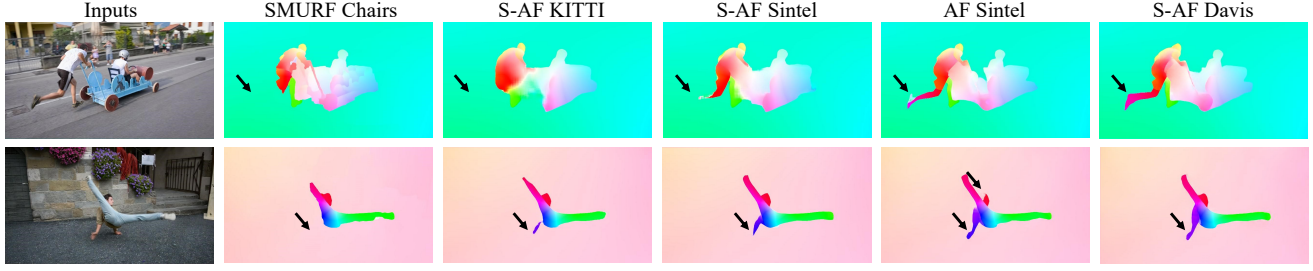


Figure 5. **Visual comparison of pre-training on DAVIS.** Compared to SMURF Chairs and AutoFlow (AF) Sintel, self-supervised AutoFlow (S-AF) DAVIS learned from DAVIS data yields better flow results. In addition, S-AF DAVIS outperforms S-AF Sintel and S-AF KITTI, indicating S-AF successfully learns a better training set to adapt the model to a target domain.

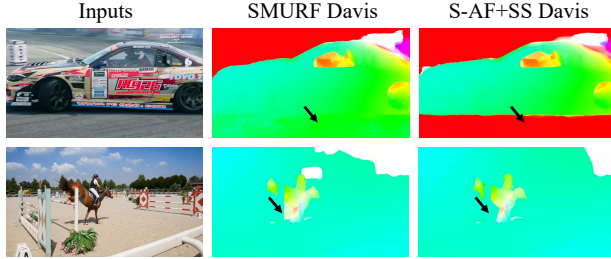


Figure 6. **Visual comparison of self-supervised fine-tuning on DAVIS.** With self-supervised fine-tuning on the target DAVIS dataset, our S-AF+SS DAVIS predicts more accurate flow for textureless areas or thin objects, showing that the better initialization of S-AF leads to better self-supervised fine-tuning results compared to the initialization from pre-training on FlyingChairs.

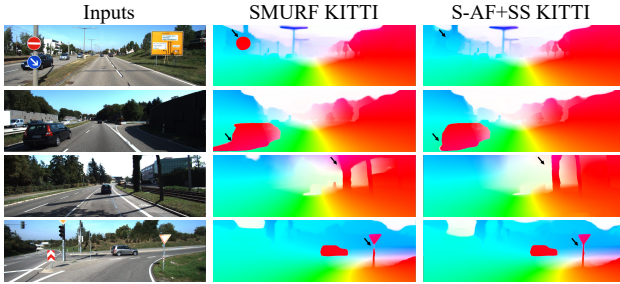


Figure 7. **Visual comparison of self-supervised fine-tuning on KITTI.** Our S-AF+SS KITTI model predicts more accurate flow on objects with large motion, on shadows, and on thin structures of the scene compared to SMURF KITTI. Purely self-supervised methods may predict incorrect flow fields, while our S-AF+SS approach resolves this issue by a better initialization.

fine-tuning; suggesting that our S-AF is complementary to the self-supervised learning approach.

**DAVIS.** Fig. 5 shows comparison of different pre-training methods on the DAVIS dataset. The SMURF Chairs model does not clearly capture the motion of the foot and hand of the person due to the domain gap between FlyingChairs

and DAVIS. AF Sintel does not generalize well to the real-world DAVIS data; our S-AF learned from the unlabeled DAVIS data successfully captures the detailed structure. We further compare our models that use different target domains for dataset generation (S-AF DAVIS, S-AF Sintel, S-AF KITTI). S-AF DAVIS shows the best results by successfully optimizing the rendering parameters for the real-world target domain, *i.e.* DAVIS.

Fig. 6 shows that self-supervised fine-tuning on DAVIS (S-AF+SS DAVIS) further improves the result over SMURF DAVIS, showing that the better initialization of S-AF leads to better self-supervised fine-tuning results compared to the initialization from pre-training on FlyingChairs.

**KITTI.** As shown in Fig. 7, S-AF+SS KITTI predicts more accurate flow on close objects with large motion, shadows, and thin structures of the scene than SMURF KITTI. The results suggest that the purely self-supervised method may predict incorrect flow due to optimizing the photometric constancy loss. In contrast, our S-AF pre-training approach provides a better model initialization and resolves this issue by pre-training on rendered S-AF data ground truth.

**Discussions.** Despite the promising results, the visual comparison suggests that there is room for improvement, such as the thin structures in Fig. 5 and the sky regions in Fig. 6. Future work may further explore using a more realistic rendering engine *e.g.*, with a sky model, and developing better self-supervised losses to address these issues.

## 5. Conclusions

We have introduced self-supervised AutoFlow to learn a training set for optical flow for unlabeled data using self-supervised metric. Self-supervised AutoFlow performs on par with AutoFlow that uses ground truth on Sintel and KITTI, and better on the real-world DAVIS dataset where ground truth is not available. Our work suggests the benefits of connecting learning to render with self-supervision and we hope to see more work in this direction to solve optical flow in the real world.



## References

- [1] Aria Ahmadi and Ioannis Patras. Unsupervised convolutional neural networks for motion estimation. In *ICIP*, 2016. 2
- [2] Filippo Aleotti, Matteo Poggi, and Stefano Mattoccia. Learning optical flow from still images. In *CVPR*, 2021. 2
- [3] Benjamin Biggs, Thomas Roddick, Andrew Fitzgibbon, and Roberto Cipolla. Creatures great and SMAL: Recovering the shape and motion of animals from video. In *ACCV*, 2018. 7
- [4] Daniel J. Butler, Jonas Wulff, Garrett B. Stanley, and Michael J. Black. A naturalistic open source movie for optical flow evaluation. In *ECCV*, 2012. 1, 2, 6, 11, 14
- [5] Mathilde Caron, Hugo Touvron, Ishan Misra, Hervé Jégou, Julien Mairal, Piotr Bojanowski, and Armand Joulin. Emerging properties in self-supervised vision transformers. In *ICCV*, 2021. 7, 12
- [6] Alexey Dosovitskiy, Philipp Fischer, Eddy Ilg, Philip Häusser, Caner Hazırbaş, Vladimir Golkov, Patrick van der Smagt, Daniel Cremers, and Thomas Brox. FlowNet: Learning optical flow with convolutional networks. In *ICCV*, 2015. 1, 2
- [7] Ian J. Goodfellow, Jean Pouget-Abadie, Mehdi Mirza, Bing Xu, David Warde-Farley, Sherjil Ozair, Aaron Courville, and Yoshua Bengio. Generative adversarial nets. In *NIPS*, 2014. 2
- [8] Klaus Greff, Francois Belletti, Lucas Beyer, Carl Doersch, Yilun Du, Daniel Duckworth, David J. Fleet, Dan Gnanaprasam, Florian Golemo, Charles Herrmann, et al. Kubric: A scalable dataset generator. In *CVPR*, 2022. 2
- [9] Yunhui Han, Kunming Luo, Ao Luo, Jiangyu Liu, Haoqiang Fan, Guiming Luo, and Shuaicheng Liu. RealFlow: EM-based realistic optical flow dataset generation from videos. In *ECCV*, 2022. 2, 6, 7, 12
- [10] Adam W. Harley, Zhaoyuan Fang, and Katerina Fragkiadaki. Particle video revisited: Tracking through occlusions using point trajectories. In *ECCV*, 2022. 7, 12
- [11] Zhaoyang Huang, Xiaoyu Shi, Chao Zhang, Qiang Wang, Ka Chun Cheung, Hongwei Qin, Jifeng Dai, and Hongsheng Li. FlowFormer: A transformer architecture for optical flow. In *ECCV*, 2022. 2
- [12] Tak-Wai Hui, Xiaoou Tang, and Chen Change Loy. LiteFlowNet: A lightweight convolutional neural network for optical flow estimation. In *CVPR*, 2018. 2
- [13] Clive Humby. Data is the new oil. *Proc. ANA Sr. Marketer's Summit*. Evanston, IL, USA, 2006. 1
- [14] Eddy Ilg, Nikolaus Mayer, Tonmoy Saikia, Margret Keuper, Alexey Dosovitskiy, and Thomas Brox. FlowNet 2.0: Evolution of optical flow estimation with deep networks. In *CVPR*, 2017. 2
- [15] Woobin Im, Tae-Kyun Kim, and Sung-Eui Yoon. Unsupervised learning of optical flow with deep feature similarity. In *ECCV*, 2020. 1, 2, 6
- [16] Woobin Im, Sebin Lee, and Sung-Eui Yoon. Semi-supervised learning of optical flow by flow supervisor. In *ECCV*, 2022. 2, 6, 7, 12
- [17] Andrew Jaegle, Sebastian Borgeaud, Jean-Baptiste Alayrac, Carl Doersch, Catalin Ionescu, David Ding, Skanda Kopula, Daniel Zoran, Andrew Brock, Evan Shelhamer, et al. Perceiver IO: A general architecture for structured inputs & outputs. In *ICLR*, 2022. 2
- [18] Azin Jahedi, Lukas Mehl, Marc Rivinius, and Andrés Bruhn. Multi-Scale RAFT: Combining hierarchical concepts for learning-based optical flow estimation. In *ICIP*, 2022. 2
- [19] Shihao Jiang, Dylan Campbell, Yao Lu, Hongdong Li, and Richard Hartley. Learning to estimate hidden motions with global motion aggregation. In *ICCV*, 2021. 2
- [20] Rico Jonschkowski, Austin Stone, Jonathan T. Barron, Ariel Gordon, Kurt Konolige, and Anelia Angelova. What matters in unsupervised optical flow. In *ECCV*, 2020. 2, 6
- [21] Alex Krizhevsky, Ilya Sutskever, and Geoffrey E. Hinton. ImageNet classification with deep convolutional neural networks. In *NIPS*, 2012. 1
- [22] Wei-Sheng Lai, Jia-Bin Huang, and Ming-Hsuan Yang. Semi-supervised learning for optical flow with generative adversarial networks. In *NIPS*, 2017. 2
- [23] Liang Liu, Jiangning Zhang, Ruifei He, Yong Liu, Yabiao Wang, Ying Tai, Donghao Luo, Chengjie Wang, Jilin Li, and Feiyue Huang. Learning by Analogy: Reliable supervision from transformations for unsupervised optical flow estimation. In *CVPR*, 2020. 1, 2, 6
- [24] Pengpeng Liu, Irwin King, Michael R. Lyu, and Jia Xu. DDFlow: Learning optical flow with unlabeled data distillation. In *AAAI*, 2019. 1, 2, 6
- [25] Pengpeng Liu, Michael R. Lyu, Irwin King, and Jia Xu. SelfFlow: Self-supervised learning of optical flow. In *CVPR*, 2019. 1, 2, 6
- [26] Nikolaus Mayer, Eddy Ilg, Philipp Fischer, Caner Hazırbaş, Daniel Cremers, Alexey Dosovitskiy, and Thomas Brox. What makes good synthetic training data for learning disparity and optical flow estimation? *IJCV*, 2018. 1, 2
- [27] Simon Meister, Junhwa Hur, and Stefan Roth. UnFlow: Unsupervised learning of optical flow with a bidirectional census loss. In *AAAI*, 2018. 2
- [28] Moritz Menze, Christian Heipke, and Andreas Geiger. Joint 3D estimation of vehicles and scene flow. In *ISPRS Workshop on Image Sequence Analysis (ISA)*, 2015. 1, 2, 6, 11, 14
- [29] Jordi Pont-Tuset, Federico Perazzi, Sergi Caelles, Pablo Arbeláez, Alexander Sorkine-Hornung, and Luc Van Gool. The 2017 DAVIS challenge on video object segmentation. *arXiv preprint arXiv:1704.00675*, 2017. 2, 7, 11
- [30] René Ranftl, Alexey Bochkovskiy, and Vladlen Koltun. Vision transformers for dense prediction. In *ICCV*, 2021. 3
- [31] René Ranftl, Katrin Lasinger, David Hafner, Konrad Schindler, and Vladlen Koltun. Towards robust monocular depth estimation: Mixing datasets for zero-shot cross-dataset transfer. *PAMI*, 2020. 3
- [32] Anurag Ranjan and Michael J. Black. Optical flow estimation using a spatial pyramid network. In *CVPR*, 2017. 2
- [33] Zhe Ren, Junchi Yan, Bingbing Ni, Bin Liu, Xiaokang Yang, and Hongyuan Zha. Unsupervised deep learning for optical flow estimation. In *AAAI*, 2017. 2

- [34] Stephan R. Richter, Zeeshan Hayder, and Vladlen Koltun. Playing for benchmarks. In *ICCV*, 2017. [2](#)
- [35] Olaf Ronneberger, Philipp Fischer, and Thomas Brox. U-Net: Convolutional networks for biomedical image segmentation. In *MICCAI*, 2015. [2](#)
- [36] Olga Russakovsky, Jia Deng, Hao Su, Jonathan Krause, Sanjeev Satheesh, Sean Ma, Zhiheng Huang, Andrej Karpathy, Aditya Khosla, Michael Bernstein, et al. ImageNet large scale visual recognition challenge. *IJCV*, 115(3):211–252, 2015. [1](#)
- [37] Leslie N. Smith and Nicholay Topin. Super-convergence: Very fast training of neural networks using large learning rates. In *Artificial intelligence and machine learning for multi-domain operations applications*, volume 11006, pages 369–386. SPIE, 2019. [4](#)
- [38] Austin Stone, Daniel Maurer, Alper Ayvaci, Anelia Angelova, and Rico Jonschkowski. SMURF: Self-teaching multi-frame unsupervised raft with full-image warping. In *CVPR*, 2021. [2](#), [3](#), [4](#), [5](#), [6](#), [7](#), [11](#), [12](#), [14](#)
- [39] Xiuchao Sui, Shaohua Li, Xue Geng, Yan Wu, Xinxing Xu, Yong Liu, Rick Goh, and Hongyuan Zhu. CRAFT: Cross-attentional flow transformer for robust optical flow. In *CVPR*, 2022. [2](#)
- [40] Deqing Sun, Charles Herrmann, Fitsum Reda, Michael Rubinstein, David J. Fleet, and William T. Freeman. Disentangling architecture and training for optical flow. In *ECCV*, 2022. [2](#), [5](#), [7](#), [12](#)
- [41] Deqing Sun, Daniel Vlasic, Charles Herrmann, Varun Jampani, Michael Krainin, Huiwen Chang, Ramin Zabih, William T. Freeman, and Ce Liu. AutoFlow: Learning a better training set for optical flow. In *CVPR*, 2021. [1](#), [2](#), [3](#), [5](#), [7](#), [12](#)
- [42] Deqing Sun, Xiaodong Yang, Ming-Yu Liu, and Jan Kautz. PWC-Net: CNNs for optical flow using pyramid, warping, and cost volume. In *CVPR*, 2018. [2](#), [3](#)
- [43] Zachary Teed and Jia Deng. RAFT: Recurrent all-pairs field transforms for optical flow. In *ECCV*, 2020. [2](#), [4](#), [5](#), [11](#)
- [44] Yang Wang, Yi Yang, Zhenheng Yang, Liang Zhao, Peng Wang, and Wei Xu. Occlusion aware unsupervised learning of optical flow. In *CVPR*, 2018. [2](#)
- [45] Taihong Xiao, Jinwei Yuan, Deqing Sun, Qifei Wang, Xinyu Zhang, Kehan Xu, and Ming-Hsuan Yang. Learnable cost volume using the cayley representation. In *ECCV*, 2020. [2](#)
- [46] Haofei Xu, Jiaolong Yang, Jianfei Cai, Juyong Zhang, and Xin Tong. High-resolution optical flow from 1D attention and correlation. In *ICCV*, 2021. [2](#)
- [47] Gengshan Yang, Deqing Sun, Varun Jampani, Daniel Vlasic, Forrester Cole, Huiwen Chang, Deva Ramanan, William T. Freeman, and Ce Liu. LASR: Learning articulated shape reconstruction from a monocular video. In *CVPR*, 2021. [7](#)
- [48] Yi Yang and Deva Ramanan. Articulated human detection with flexible mixtures of parts. *PAMI*, 35(12):2878–2890, 2012. [7](#)
- [49] Yanchao Yang and Stefano Soatto. Conditional prior networks for optical flow. In *ECCV*, 2018. [2](#)
- [50] Jason J. Yu, Adam W. Harley, and Konstantinos G. Derpanis. Back to Basics: Unsupervised learning of optical flow via brightness constancy and motion smoothness. In *ECCVW*, 2016. [2](#)
- [51] Shuai Yuan, Xian Sun, Hannah Kim, Shuzhi Yu, and Carlo Tomasi. Optical flow training under limited label budget via active learning. In *ECCV*, 2022. [2](#)
- [52] Ramin Zabih and John Woodfill. Non-parametric local transforms for computing visual correspondence. In *ECCV*, 1994. [4](#)
- [53] Feihu Zhang, Oliver J. Woodford, Victor Adrian Prisacariu, and Philip H.S. Torr. Separable flow: Learning motion cost volumes for optical flow estimation. In *ICCV*, 2021. [2](#)
- [54] Yiran Zhong, Pan Ji, Jianyuan Wang, Yuchao Dai, and Hongdong Li. Unsupervised deep epipolar flow for stationary or dynamic scenes. In *CVPR*, 2019. [1](#), [2](#), [6](#)

## Appendix

### A. Implementation Details

**Training details.** We use 80k training steps for the rendering hyperparameter search. We include the following rendering hyperparameters for generating the S-AF data:

- Number of foreground objects
- Scale, rotation, translation, grid strength, grid size of the motion for foreground
- Scale, rotation, translation, grid strength, grid size of the motion for background
- Probability and strength of the mask blur
- Probability and strength of the motion blur
- Probability, density and brightness of the fog
- Minimum and maximum of the object’s diagonal
- Minimum and maximum of the object’s center location
- Irregularity and spikiness of the polygon

As for the hyperparameters in the search metric Eq. (2) in the main paper, we use  $(w_{\text{smooth}}, w_{\text{distill}})=(0.6, 4)$  for the Sintel [4] and the DAVIS dataset [29], and  $(w_{\text{smooth}}, w_{\text{distill}})=(1.2, 8)$  for the KITTI dataset [28]. We pretrain the model on a generated S-AF dataset  $\mathbf{D}_{\text{auto}}$  for 3.2 M iterations for Sintel and 200 k iterations for KITTI and DAVIS. We randomly crop input images to size  $368 \times 496$  at training time and use a batch size of 36.

We further fine-tune the model with the self-supervised loss (Eq. (3)) for 12 k iterations on the Sintel dataset, 75 k iterations on the KITTI dataset, and 100 k iterations on the Davis dataset. We further apply the multi-frame fine-tuning on Sintel and KITTI datasets for 30 k iterations (Eq. (4)) with the same parameter setting from SMURF [38]. We randomly crop input images to size  $368 \times 496$  at training time and use a batch size of 8. We use the data augmentations from RAFT [43] including random cropping, stretching, scaling, flipping, and erasing. As for the photometric augmentations, we randomly adjust the contrast, saturation, brightness and hue.

**Evaluation metrics.** We use the average end-point error (AEPE) evaluation metric. For KITTI, we additionally report the outlier rate (FI-all), *i.e.* the ratio (in %) of outlier pixels among all ground truth pixels. If an error of a pixel exceeds the 3-pixel threshold and 5% w.r.t. the ground truth, the pixel is considered as an outlier.

### B. Ablation Studies

#### B.1. Training by individual S-AF dataset and mixed S-AF dataset

As described in Sec. 3.2 and Sec. 4.2, to improve the robustness of the algorithm, we sort the sets of hyperparameters returned by Self-AutoFlow according to the self-supervised search metric and choose the top-3 hyperparameter sets. We form our final Self-AutoFlow dataset by equally mixing a set of images generated from each hyperparameter set. For a fair comparison, we also prepare an equivalent model for AutoFlow, denoted as AF-mix. In addition to the results of training on the dataset generated by mixing the top-3 hyperparameters in Tab. 1, we report the results of training models on each individual S-AF and AF dataset in Tab. 6. The models are trained for 0.2M iterations. We note that the top hyperparameters sets are selected according to the search, where the model is trained for 40K iterations, and here we report the results of model trained for 0.2M iterations, so the top-1 hyperparameters might not have the lowest AEPE for AF models.

Unlike supervised AutoFlow, the results of S-AF trained on the top-2 hyperparameters on Sintel Final and S-AF trained on the top-3 hyperparameters on KITTI show that there is no guarantee that the top candidates returned by self-supervised AutoFlow are the optimal set of hyperparameters. Mixing the top-3 datasets decreases the likelihood of sampling a poor-performing AutoFlow hyperparameters and improves the robustness of the algorithm.

Table 6. **Training by individual S-AF dataset and mixed S-AF dataset.** We show that training on mix-3 datasets decreases the likelihood of sampling a poor-performing AutoFlow hyperparameters and improves the robustness of the algorithm.

Method	Sintel Clean [4]				Sintel Final [4]				KITTI 2015 [28]			
	top-1	top-2	top-3	mix-3	top-1	top-2	top-3	mix-3	top-1	top-2	top-3	mix-3
AF-mix (0.2M)	2.11	2.18	2.10	2.18	2.85	2.83	2.82	2.83	4.70	4.35	4.58	4.43
S-AF (0.2M)	2.16	2.14	2.13	2.22	2.83	<b>2.93</b>	2.84	2.84	4.65	4.06	<b>5.40</b>	4.58

## B.2. Keypoint propagation on BADJA including occluded keypoints

As described in Sec. 4.5, we report the accuracy of keypoint propagation on BADJA sequences using (semi-)supervised and self-supervised optical flow methods. We discard the dog-agility sequence and exclude all keypoints once they become occluded for a reliable optical flow evaluation. In Tab. 7, we provide the keypoint propagation accuracy including the dog-agility sequence and the occluded keypoints. Tab. 7 shows similar conclusion as Tab. 5.

Table 7. **Keypoint propagation on BADJA.** In the main paper, we discard the dog-a sequence and exclude all keypoints once they become occluded for a better judgement on optical-flow-based methods. Here we include the full results with dog-a sequence and evaluation of invisible keypoints for reference.

Method	bear	camel	cows	dog-a	dog	horse-h	horse-l	Avg.
DINO [5]	75.7	58.2	71.4	10.3	46.0	35.8	56.5	50.6
PIPs [10]	76.3	84.0	79.1	31.6	42.9	60.4	58.6	<b>61.8</b>
<b>(Semi-)supervised</b>								
SemiFlow-Davis [16]	66.4	72.0	71.4	13.8	40.8	36.4	31.4	47.5
RealFlow-Davis [9]	64.3	80.1	63.4	10.3	45.4	32.5	38.7	47.8
AF Sintel [41]	71.4	80.1	75.1	17.2	47.1	34.4	27.2	50.4
RAFT-it [40]	73.2	83.0	78.1	17.2	46.0	39.1	30.4	<b>52.4</b>
<b>Pre-training</b>								
SMURF Chairs [38]	79.3	74.0	73.8	3.4	42.5	34.4	29.3	48.1
S-AF Sintel	73.2	83.9	62.0	3.4	42.0	40.4	26.7	47.4
S-AF KITTI	72.5	76.8	73.8	0.0	46.6	34.4	31.9	48.0
S-AF DAVIS	72.9	76.5	75.7	20.7	47.7	38.4	31.4	<b>51.9</b>
<b>Self-supervised fine-tuning</b>								
SMURF DAVIS [38]	80.0	83.0	77.8	3.4	47.1	40.4	44.0	53.7
S-AF+SS DAVIS	80.0	82.3	74.9	10.3	50.6	43.0	42.4	<b>54.8</b>

In Fig. 8, we show an example of the occluded keypoint. We note that the gray keypoint on the left rear foot is occluded by the right rear foot in the second frame. Therefore, by the definition of optical flow, the keypoint should be propagated to the position of the right foot in the third frame, and the prediction shown in the figure is correct. However, by the definition of keypoints, the gray dot should be attached to the left foot in the third frame, and thus the prediction shown is an error. Based on this observation, we exclude a keypoint once it becomes invisible (which is provided in the annotations), to better evaluate the optical-flow-based methods and reduce noises in the evaluations.



Figure 8. **Occluded keypoints.** The gray keypoint on the left rear foot is occluded by the right rear foot in the second frame. Afterward, the gray keypoint is attached to the right rear foot, which is an error for keypoint propagation but it is correct by the definition of optical flow.

## B.3. Sequence losses in the search metric of S-AF

In Sec. 3.2, we mention that since there is no backpropagation to the model in the search of AutoFlow, the search metric uses only the final flow prediction of RAFT instead of all intermediate. In Fig. 9, we conduct a study of using the intermediate predictions of RAFT to compute the search metric. Specifically, we compute the search metric once for each intermediate prediction and we exponentially decay the weight for earlier predictions [38]. Since the search metric is computed at the original resolution of the target data, we use at most the last four predictions due to memory constraints.

We conduct the S-AF search using last-1 prediction (ours), last-2 prediction and last-4 prediction as the search metric. We report the average AEPE of the top-3 models selected by the search metric. The models are trained for 40k iterations in the



search. Empirically, we find that using the intermediate predictions in the search metric results in a higher AEPE and does not improve the S-AF search.

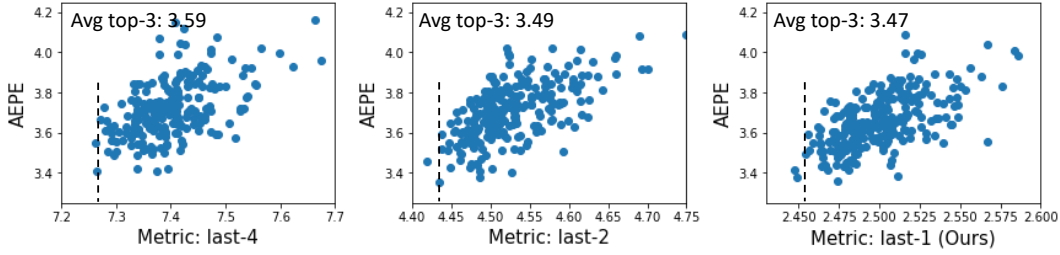


Figure 9. **Sequence losses.** We find that using the intermediate predictions of RAFT to compute the search metric does not lead to a better set of S-AF hyperparameters.

## C. Analysis and Discussion

### C.1. Motion statistics of S-AF and AF

We compute the statistics of the motion magnitude of the generated optical flow ground truth in S-AF and AF datasets in Fig. 10. We find that when the target dataset is Sintel, the motion statistics of S-AF are similar to the statistics of Sintel data. In contrast, the motion statistics of AutoFlow are different from the Sintel data. In addition, S-AF focuses more on the small motion compared to AF which focuses on middle-range motion. We hypothesize that the self-supervised search metric may have much smaller values for middle/high-range motions compared to AEPE which penalizes significantly on the error at the regions of large motions. Therefore, the S-AF data does not focus on regions with large motions compared to AF. Similar to Tab. 6, we also show the statistics of each individual S-AF dataset and the mixed dataset. We find the statistics are similar for each individual S-AF data.

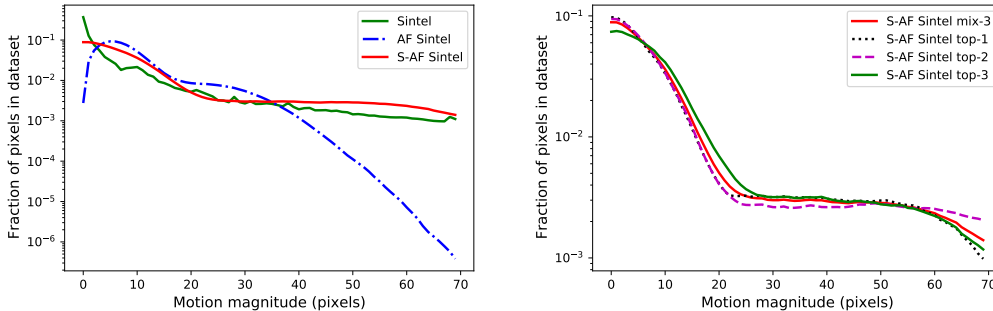


Figure 10. **Histogram of motion magnitude.** We include the motion statistics of the generated flow field by Self-AutoFlow and AutoFlow. Interestingly, the Self-AutoFlow data focuses more on small motion compared to AutoFlow. Also, the statistics of Self-AutoFlow are closer to the statistics of Sintel data. In addition, we show the statistics of individual S-AF dataset and their mixed results.

### C.2. AEPE versus self-supervised losses of SMURF and S-AF

We calculate the self-supervised losses and the AEPE on the target datasets for SMURF and S-AF models in Tab. 8. The losses and errors are computed for the full target datasets and we report the average. In most cases, the SMURF models have a lower self-supervised losses compared to the S-AF models, while the S-AF models have lower AEPE.

Although the self-supervised metric is highly correlated with the AEPE, optimizing it *directly* by backpropagation to the model might lead to a model with lower self-supervised loss and higher EPE. In contrast, our Self-AutoFlow method uses the self-supervised loss *indirectly* to assess the quality of a generated dataset, which results in a model with higher self-supervised loss and lower EPE. To conclude, Self-AutoFlow is a good strategy for using self-supervised losses.

Table 8. **Self-supervised losses versus AEPE.** We compute the photometric, distillation and smoothness loss averaged on the training set. We show that our S-AF model which uses the self-supervised loss *indirectly* to assess the quality of a generated dataset results in a model with higher self-supervised loss and lower EPE.

Method	Sintel Final [4]					KITTI 2015 [28]				
	$\mathcal{L}_{\text{photo}} \downarrow$	$\mathcal{L}_{\text{distill}} \downarrow$	$\mathcal{L}_{\text{smooth}} \downarrow$	$\mathcal{L}_{\text{total}} \downarrow$	$AEPE \downarrow$	$\mathcal{L}_{\text{photo}} \downarrow$	$\mathcal{L}_{\text{distill}} \downarrow$	$\mathcal{L}_{\text{smooth}} \downarrow$	$\mathcal{L}_{\text{total}} \downarrow$	$AEPE \downarrow$
SMURF Chairs [38]	2.20	0.70	<b>0.013</b>	2.92	3.35	2.61	<b>1.05</b>	<b>0.0046</b>	<b>3.67</b>	7.94
S-AF	2.20	<b>0.44</b>	0.017	<b>2.66</b>	<b>2.57</b>	<b>2.54</b>	1.24	0.0052	3.78	<b>4.28</b>
+SS Sintel/KITTI										
SMURF [38]	<b>2.17</b>	0.67	<b>0.012</b>	<b>2.86</b>	2.80	2.54	<b>0.80</b>	0.0046	<b>3.35</b>	2.01
S-AF	2.20	<b>0.65</b>	0.013	2.87	<b>2.40</b>	<b>2.49</b>	0.87	<b>0.0043</b>	3.37	<b>1.94</b>

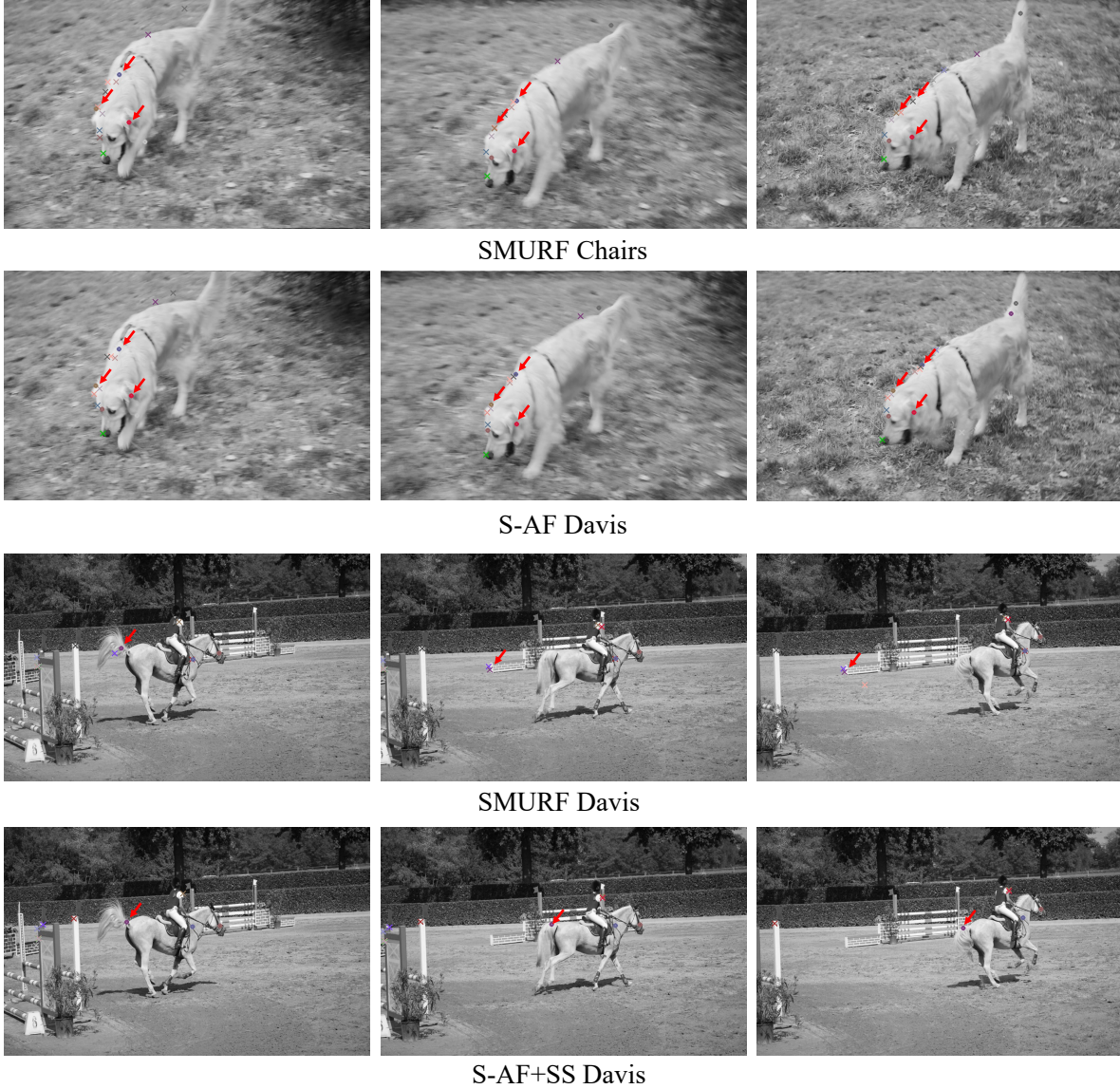


Figure 11. **Visual results of keypoints on BADJA.** The keypoints correctly tracked are marked as a dot, and the keypoints with the wrong trajectory are marked as a cross. Compared the results without self-supervised fine-tuning in (a), S-AF track the three keypoints (gray, red, and brown) correctly, while SMURF loses the brown keypoint in the second frame and the gray keypoint in the third frame. As for the results with self-supervised fine-tuning, S-AF correctly tracks the purple keypoint on the tail, and SMURF loses it since the second frame.

Table 9. Detailed performance of S-AF+SS on public benchmark.

Model	all	match	unmatch	d0-10	d10-60	d60-140	s0-10	s10-40	s40+
SMURF	3.15	1.55	16.23	3.14	1.31	0.86	0.40	1.37	21.15
S-AF+SS	3.03	1.12	18.58	2.58	0.99	0.58	0.41	1.19	20.48

(a) Sintel Clean

Model	all	match	unmatch	d0-10	d10-60	d60-140	s0-10	s10-40	s40+
SMURF	4.18	2.14	20.86	4.20	1.74	1.30	0.74	2.30	25.82
S-AF+SS	3.98	1.89	21.01	4.00	1.58	1.08	0.89	2.23	23.53

(b) Sintel Final

Model	Fl-bg	All Fl-fg	Fl-all	Fl-bg	Occ Fl-fg	Fl-all
SMURF	6.04 %	10.75 %	6.83 %	4.46 %	8.86 %	5.26 %
S-AF+SS	5.90 %	11.09 %	6.76 %	4.41 %	8.67 %	5.18 %

(c) KITTI

Table 10. Detailed performance of the supervised fine-tuning results of S-AF on public benchmark.

Model	all	match	unmatch	d0-10	d10-60	d60-140	s0-10	s10-40	s40+
RAFT-it	1.55	0.61	9.24	1.66	0.51	0.27	0.29	0.97	9.26
RAFT-S-AF	1.42	0.54	8.65	1.50	0.45	0.21	0.26	0.90	8.46

(a) Sintel Clean

Model	all	match	unmatch	d0-10	d10-60	d60-140	s0-10	s10-40	s40+
RAFT-it	2.90	1.41	15.03	2.81	1.16	0.88	0.51	1.70	17.62
RAFT-S-AF	2.99	1.52	14.98	2.87	1.26	1.01	0.48	1.69	18.60

(b) Sintel Final

Model	Fl-bg	All Fl-fg	Fl-all	Fl-bg	Occ Fl-fg	Fl-all
RAFT-it	4.11 %	5.34 %	4.31 %	2.68 %	2.77 %	2.70 %
RAFT-S-AF	3.86 %	5.38 %	4.12 %	2.52 %	2.86 %	2.59 %

(c) KITTI

## D. Additional Results

### D.1. Visualization of keypoint propagation on BADJA

We visualize the keypoint propagation results on BADJA sequences by SMURF and our S-AF in Fig. 11. The keypoints correctly propagated are marked as a dot, and the keypoints with the wrong predicted trajectory are marked as a cross. Compared the results without self-supervised fine-tuning, S-AF tracks the three keypoints on the back (gray), left ear (red), and right ear (brown) correctly. On the other hand, SMURF loses the keypoint on the right ear (brown) since the second frame and loses the keypoint on the back (gray) since the third frame in the dog sequence. As for the models with self-supervised fine-tuning, we show the keypoint in the horsejump-low sequence. S-AF correctly predicts the trajectory of the purple keypoint on the tail, while SMURF loses it since the second frame.

### D.2. Benchmark results

We provide the screenshots of both models on the public benchmarks in Fig. 12 and Fig. 13. As listed in Tab. 2, we provide the detailed performance of our S-AF+SS models on public benchmarks in Tab. 9. The S-AF+SS model is more accurate in most cases while less accurate on unmatch and s0-10 for Sintel benchmark, and on Fl-fg all for KITTI benchmark compared to SMURF. As shown in Tab. 4, we show the detailed performance of the supervised fine-tuning model RAFT-S-AF in Tab. 10. For KITTI benchmark, RAFT-S-AF is more accurate in most cases while less accurate for Fl-fg. RAFT-S-AF is more accurate for all cases for Sintel Clean, and the cases of unmatch, s0-10, s10-40 for Sintel Final.

SfM-PM <sup>[116]</sup>	2.910	1.016	18.357	2.797	0.756	0.479	0.559	1.732	17.431	<a href="#">Visualize Results</a>
FlowFields++ <sup>[117]</sup>	2.943	0.850	20.027	2.550	0.603	0.403	0.560	1.859	17.401	<a href="#">Visualize Results</a>
GCA-Net <sup>[118]</sup>	2.947	1.032	18.585	2.900	0.830	0.456	0.602	1.645	17.753	<a href="#">Visualize Results</a>
LiteFlowNet3 <sup>[119]</sup>	2.994	1.148	18.077	3.000	0.985	0.498	0.559	1.670	18.302	<a href="#">Visualize Results</a>
ricom20201202 <sup>[120]</sup>	3.002	1.150	18.125	2.915	0.911	0.609	0.723	1.949	16.869	<a href="#">Visualize Results</a>
risc <sup>[121]</sup>	3.005	1.150	18.147	2.930	0.908	0.607	0.721	1.957	16.885	<a href="#">Visualize Results</a>
RAFT-SA <sup>[122]</sup>	3.026	1.122	18.578	2.577	0.988	0.579	0.410	1.191	20.477	<a href="#">Visualize Results</a>
LiteFlowNet3-S <sup>[123]</sup>	3.028	1.173	18.182	3.079	0.996	0.527	0.574	1.646	18.566	<a href="#">Visualize Results</a>
RICBCDN <sup>[124]</sup>	3.080	1.212	18.319	3.241	0.945	0.577	0.724	2.077	17.197	<a href="#">Visualize Results</a>
FlowFields+ <sup>[125]</sup>	3.102	0.820	21.718	2.340	0.616	0.373	0.593	1.865	18.549	<a href="#">Visualize Results</a>
DIP-Flow <sup>[126]</sup>	3.103	0.881	21.227	2.574	0.681	0.419	0.548	1.801	18.979	<a href="#">Visualize Results</a>
PST <sup>[127]</sup>	3.110	0.942	20.809	2.759	0.664	0.378	0.635	2.069	17.919	<a href="#">Visualize Results</a>
MPiF <sup>[128]</sup>	3.111	1.134	19.218	3.070	0.939	0.523	0.616	1.980	18.220	<a href="#">Visualize Results</a>
LSM_FLOW_RVC <sup>[129]</sup>	3.142	1.395	17.394	2.557	1.091	0.873	0.361	1.202	21.652	<a href="#">Visualize Results</a>
SMURF <sup>[130]</sup>	3.152	1.550	16.233	3.141	1.310	0.858	0.398	1.371	21.152	<a href="#">Visualize Results</a>

(a) Sintel Clean

RAFT+ConvUp <sup>[93]</sup>	3.642	1.661	19.796	3.372	1.258	1.096	0.732	2.054	21.920	<a href="#">Visualize Results</a>
CVPR-1235 <sup>[94]</sup>	3.649	1.912	17.818	3.857	1.576	1.144	0.823	2.965	19.311	<a href="#">Visualize Results</a>
DCVNet <sup>[95]</sup>	3.655	1.986	17.243	3.822	1.556	1.296	0.772	2.409	20.937	<a href="#">Visualize Results</a>
StaRFlow <sup>[96]</sup>	3.707	1.838	18.946	3.618	1.439	1.122	0.744	2.018	22.491	<a href="#">Visualize Results</a>
C-RAFT_RVC <sup>[97]</sup>	3.795	1.919	19.089	3.591	1.660	1.236	0.674	2.369	22.723	<a href="#">Visualize Results</a>
Flow1D <sup>[98]</sup>	3.806	1.949	18.946	3.604	1.756	1.394	0.738	2.479	22.221	<a href="#">Visualize Results</a>
RAFT-SA <sup>[99]</sup>	3.977	1.889	21.005	3.995	1.575	1.077	0.889	2.234	23.527	<a href="#">Visualize Results</a>
IOFPL-CVr8-ft <sup>[100]</sup>	4.014	1.906	21.194	3.246	1.418	1.374	0.656	1.905	25.767	<a href="#">Visualize Results</a>
ADW-Net <sup>[101]</sup>	4.017	1.951	20.855	3.720	1.472	1.308	0.818	2.442	23.694	<a href="#">Visualize Results</a>
DistillFlow+ft <sup>[102]</sup>	4.095	2.031	20.934	4.300	1.666	1.236	0.673	2.448	25.068	<a href="#">Visualize Results</a>
ScopeFlow <sup>[103]</sup>	4.098	1.999	21.214	4.028	1.689	1.180	0.725	2.589	24.477	<a href="#">Visualize Results</a>
ARFlow-mv-ft <sup>[104]</sup>	4.142	2.082	20.937	4.056	1.707	1.300	0.706	2.366	25.475	<a href="#">Visualize Results</a>
vcn+MSDRNet <sup>[105]</sup>	4.143	1.999	21.621	3.932	1.637	1.266	0.763	2.387	25.165	<a href="#">Visualize Results</a>
LSM_FLOW_RVC <sup>[106]</sup>	4.150	2.018	21.531	3.470	1.600	1.478	0.606	1.840	27.323	<a href="#">Visualize Results</a>
MaskFlowNet <sup>[107]</sup>	4.172	2.048	21.494	3.783	1.745	1.310	0.592	2.389	26.253	<a href="#">Visualize Results</a>
SMURF <sup>[108]</sup>	4.183	2.138	20.861	4.198	1.744	1.296	0.740	2.302	25.819	<a href="#">Visualize Results</a>

(b) Sintel Final

100	VCN	<a href="#">code</a>	5.83 %	8.66 %	6.30 %	100.00 %	0.18 s	Titan X Pascal	<input type="checkbox"/>
G. Yang and D. Ramanan: <a href="#">Volumetric Correspondence Networks for Optical Flow</a> . NeurIPS 2019.									
101	Stereo expansion	<a href="#">code</a>	5.83 %	8.66 %	6.30 %	100.00 %	2 s	GPU @ 2.5 Ghz (Python)	<input type="checkbox"/>
G. Yang and D. Ramanan: <a href="#">Upgrading Optical Flow to 3D Scene Flow through Optical Expansion</a> . CVPR 2020.									
102	Binary TTC	<a href="#">code</a>	5.84 %	8.67 %	6.31 %	100.00 %	2 s	GPU @ 1.0 Ghz (Python)	<input type="checkbox"/>
A. Badki, O. Gallo, J. Kautz and P. Sen: <a href="#">Binary TTC: A Temporal Geofence for Autonomous Navigation</a> . The IEEE Conference on Computer Vision and Pattern Recognition (CVPR) 2021.									
103	MonoComb	<a href="#">code</a>	5.84 %	8.67 %	6.31 %	100.00 %	0.58 s	RTX 2080 Ti	<input type="checkbox"/>
R. Schuster, C. Unger and D. Stricker: <a href="#">MonoComb: A Sparse-to-Dense Combination Approach for Monocular Scene Flow</a> . ACM Computer Science in Cars Symposium (CSCS) 2020.									
104	HD <sup>3</sup> -Flow	<a href="#">code</a>	6.05 %	9.02 %	6.55 %	100.00 %	0.10 s	NVIDIA Pascal Titan XP	<input type="checkbox"/>
Z. Yin, T. Darrell and F. Yu: <a href="#">Hierarchical Discrete Distribution Decomposition for Match Density Estimation</a> . CVPR 2019.									
105	PRSM	<a href="#">code</a>	5.33 %	13.40 %	6.68 %	100.00 %	300 s	1 core @ 2.5 Ghz (C/C++)	<input type="checkbox"/>
C. Vogel, K. Schindler and S. Roth: <a href="#">3D Scene Flow Estimation with a Piecewise Rigid Scene Model</a> . ijcv 2015.									
106	RAFT-SA	<a href="#">code</a>	5.90 %	11.09 %	6.76 %	100.00 %	1 s	1 core @ 2.5 Ghz (C/C++)	<input type="checkbox"/>
107	MaskFlowNet-S	<a href="#">code</a>	6.53 %	8.21 %	6.81 %	100.00 %	0.03 s	NVIDIA TITAN Xp	<input type="checkbox"/>
S. Zhao, Y. Sheng, Y. Dong, E. Chang and Y. Xu: <a href="#">MaskFlowNet: Asymmetric Feature Matching with Learnable Occlusion Mask</a> . Proceedings of the IEEE Conference on Computer Vision and Pattern Recognition (CVPR) 2020.									
108	ScopeFlow	<a href="#">code</a>	6.72 %	7.36 %	6.82 %	100.00 %	-1 s	Nvidia GPU	<input type="checkbox"/>
A. Bar-Haim and L. Wolf: <a href="#">ScopeFlow: Dynamic Scene Scoping for Optical Flow</a> . The IEEE Conference on Computer Vision and Pattern Recognition (CVPR) 2020.									
109	SMURF	<a href="#">code</a>	6.04 %	10.75 %	6.83 %	100.00 %	.2 s	1 core @ 2.5 Ghz (C/C++)	<input type="checkbox"/>
A. Stone, D. Maurer, A. Ayvaci, A. Angelova and R. Jonschkowski: <a href="#">SMURF: Self-Teaching Multi-Frame Unsupervised RAFT With Full-Image Warping</a> . Proceedings of the IEEE/CVF Conference on Computer Vision and Pattern Recognition (CVPR) 2021.									
110	RAFT-VM		6.49 %	8.65 %	6.85 %	100.00 %	0.4 s	GPU @ 2.5 Ghz (C/C++)	<input type="checkbox"/>
111	OSF+TC	<a href="#">code</a>	5.76 %	13.31 %	7.02 %	100.00 %	50 min	1 core @ 2.5 Ghz (C/C++)	<input type="checkbox"/>
M. Neoral and J. Sochman: <a href="#">Object Scene Flow with Temporal Consistency</a> . 22nd Computer Vision Winter Workshop (CVWW) 2017.									
112	IRR-full		6.99 %	7.57 %	7.09 %	100.00 %	0.2 s	1 core @ 2.5 Ghz (Python)	<input type="checkbox"/>

(c) KITTI

Figure 12. Screenshot of S-AF+SS on public benchmark. Our method was temporarily named as RAFT-SA.



GMA <sup>[19]</sup>	1.388	0.582	7.963	1.537	0.461	0.278	0.331	0.963	7.662	<a href="#">Visualize Results</a>
GMFlowNet <sup>[20]</sup>	1.390	0.520	8.486	1.275	0.395	0.293	0.314	0.991	7.698	<a href="#">Visualize Results</a>
GMA+LCT-Flow <sup>[21]</sup>	1.408	0.525	8.611	1.428	0.404	0.251	0.279	0.876	8.299	<a href="#">Visualize Results</a>
AGF-Flow3 <sup>[22]</sup>	1.409	0.525	8.618	1.433	0.403	0.250	0.278	0.878	8.303	<a href="#">Visualize Results</a>
RFPM <sup>[23]</sup>	1.411	0.494	8.884	1.335	0.400	0.221	0.273	0.879	8.345	<a href="#">Visualize Results</a>
RAFT-OCTC <sup>[24]</sup>	1.419	0.541	8.574	1.455	0.442	0.242	0.301	0.940	8.118	<a href="#">Visualize Results</a>
RAFT-SA+ <sup>[25]</sup>	1.421	0.535	8.654	1.495	0.451	0.207	0.260	0.896	8.460	<a href="#">Visualize Results</a>
GMA-FS <sup>[26]</sup>	1.430	0.602	8.171	1.579	0.470	0.263	0.333	0.977	7.961	<a href="#">Visualize Results</a>
AGFlow <sup>[27]</sup>	1.431	0.559	8.541	1.501	0.452	0.261	0.319	0.963	8.075	<a href="#">Visualize Results</a>
DIP <sup>[28]</sup>	1.435	0.519	8.919	1.102	0.407	0.312	0.336	0.754	8.546	<a href="#">Visualize Results</a>
CRAFT <sup>[29]</sup>	1.441	0.611	8.204	1.574	0.552	0.249	0.311	0.991	8.131	<a href="#">Visualize Results</a>
ErrorMatch-GMA <sup>[30]</sup>	1.446	0.584	8.472	1.503	0.483	0.280	0.311	0.935	8.314	<a href="#">Visualize Results</a>
GMA-base <sup>[31]</sup>	1.450	0.591	8.440	1.532	0.470	0.280	0.321	0.951	8.251	<a href="#">Visualize Results</a>

(a) Sintel Clean

FCTR <sup>[57]</sup>	2.927	1.291	16.270	2.811	1.100	0.780	0.562	1.633	17.800	<a href="#">Visualize Results</a>
SSTM++nws <sup>[58]</sup>	2.931	1.271	16.472	2.917	1.076	0.648	0.511	1.660	18.022	<a href="#">Visualize Results</a>
SwinTR-RAFT <sup>[59]</sup>	2.946	1.411	15.457	2.676	1.045	0.983	0.513	1.640	18.175	<a href="#">Visualize Results</a>
L2L-Flow-ext <sup>[60]</sup>	2.954	1.392	15.684	3.059	1.158	0.822	0.649	1.823	17.125	<a href="#">Visualize Results</a>
AGM-FlowNet <sup>[61]</sup>	2.959	1.333	16.210	2.670	0.996	0.824	0.550	1.674	18.014	<a href="#">Visualize Results</a>
MF2C <sup>[62]</sup>	2.980	1.484	15.191	3.187	1.281	0.978	0.692	2.060	16.560	<a href="#">Visualize Results</a>
RAFT-SA+ <sup>[63]</sup>	2.989	1.518	14.981	2.865	1.255	1.012	0.477	1.686	18.598	<a href="#">Visualize Results</a>
RAFT+LCT-Flow <sup>[64]</sup>	3.024	1.381	16.428	2.650	1.041	0.944	0.519	1.603	18.898	<a href="#">Visualize Results</a>
CSFlow-2-view <sup>[65]</sup>	3.025	1.445	15.914	3.061	1.125	0.877	0.622	1.881	17.720	<a href="#">Visualize Results</a>
AGF-Flow2 <sup>[66]</sup>	3.028	1.385	16.430	2.653	1.043	0.951	0.527	1.602	18.899	<a href="#">Visualize Results</a>
MFFC <sup>[67]</sup>	3.029	1.517	15.363	3.135	1.189	0.916	0.621	1.812	17.929	<a href="#">Visualize Results</a>
RAFT-DFlow <sup>[68]</sup>	3.065	1.453	16.212	3.028	1.115	0.885	0.617	1.907	18.019	<a href="#">Visualize Results</a>
SSTM-nws <sup>[69]</sup>	3.076	1.431	16.491	2.992	1.129	0.843	0.553	1.935	18.356	<a href="#">Visualize Results</a>
RAFT+OBS <sup>[70]</sup>	3.104	1.487	16.286	3.107	1.153	0.964	0.657	1.940	18.061	<a href="#">Visualize Results</a>
RAFT-A <sup>[71]</sup>	3.137	1.590	15.762	3.153	1.270	1.032	0.534	1.956	18.912	<a href="#">Visualize Results</a>

(b) Sintel Final

4	<a href="#">RigidMask-ISF</a>	<a href="#">code</a>	2.63 %	7.85 %	3.50 %	100.00 %	3.3 s	GPU @ 2.5 Ghz (Python)	<input type="checkbox"/>
G. Yang and D. Ramanan: <a href="#">Learning to Segment Rigid Motions from Two Frames</a> . CVPR 2021.									
5	<a href="#">TPCV-RAFT3D</a>	<a href="#">code</a>	2.48 %	10.19 %	3.76 %	100.00 %	0.2 s	1 core @ 2.5 Ghz (C/C++)	<input type="checkbox"/>
6	<a href="#">RAFT-it+ RVC</a>	<a href="#">code</a>	3.62 %	5.33 %	3.90 %	100.00 %	0.14 s	1 core @ 2.5 Ghz (Python)	<input type="checkbox"/>
7	<a href="#">RAFT-OCTC</a>	<a href="#">code</a>	3.72 %	5.39 %	4.00 %	100.00 %	0.2 s	GPU @ 2.5 Ghz (Python)	<input type="checkbox"/>
J. Jeong, J. Lin, F. Porikli and N. Kwak: <a href="#">Imposing Consistency for Optical Flow Estimation (Qualcomm AI Research)</a> . CVPR 2022.									
8	<a href="#">SF2SE3</a>	<a href="#">code</a>	3.17 %	8.79 %	4.11 %	100.00 %	2.7 s	GPU @ >3.5 Ghz (Python)	<input type="checkbox"/>
L. Sommer, P. Schröppel and T. Brox: <a href="#">SF2SE3: Clustering Scene Flow into SE (3)-Motions via Proposal and Selection</a> . DAGM German Conference on Pattern Recognition 2022.									
9	<a href="#">RAFT-CF-PL3</a>	<a href="#">code</a>	3.80 %	5.65 %	4.11 %	100.00 %	0.05 s	GPU @ 2.5 Ghz (Python)	<input type="checkbox"/>
Z. Zhang, P. Ji, N. Bansal, C. Cai, Q. Yan, X. Xu and Y. Xu: <a href="#">CLIP-Flow: Contrastive Learning by semi-supervised Iterative Pseudo Labeling for Optical Flow Estimation</a> . 2022.									
10	<a href="#">RAFT-S-AF</a>	<a href="#">code</a>	3.86 %	5.38 %	4.12 %	100.00 %	1 s	1 core @ 2.5 Ghz (C/C++)	<input type="checkbox"/>
11	<a href="#">MS RAFT+ corr RVC</a>	<a href="#">code</a>	3.83 %	5.71 %	4.15 %	100.00 %	0.65 s	GPU @ 2.5 Ghz (Python + C/C++)	<input type="checkbox"/>
A. Jahedi, M. Luz, L. Mehl, M. Rivinius and A. Bruhn: <a href="#">High Resolution Multi-Scale RAFT</a> . Robust Vision Challenge 2022, arXiv preprint arXiv:2210.16900 2022.									
A. Jahedi, L. Mehl, M. Rivinius and A. Bruhn: <a href="#">Multi-Scale Raft: Combine Hierarchical Concepts for Learning-Based Optical Flow Estimation</a> . IEEE International Conference on Image Processing (ICIP) 2022.									
12	<a href="#">MS RAFT+ RVC</a>	<a href="#">code</a>	3.89 %	5.67 %	4.19 %	100.00 %	0.65 s	GPU @ 2.5 Ghz (Python + C/C++)	<input type="checkbox"/>
13	<a href="#">DIP</a>	<a href="#">code</a>	3.86 %	5.96 %	4.21 %	100.00 %	0.15 s	1 core @ 2.5 Ghz (Python)	<input type="checkbox"/>
Z. Zheng, N. Nie, Z. Ling, P. Xiong, J. Liu, H. Wang and J. Li: <a href="#">DIP: Deep Inverse Patchmatch for High-Resolution Optical Flow</a> . Proceedings of the IEEE/CVF Conference on Computer Vision and Pattern Recognition 2022.									
14	<a href="#">RAFT-3D</a>	<a href="#">code</a>	3.39 %	8.79 %	4.29 %	100.00 %	2 s	GPU @ 2.5 Ghz (Python + C/C++)	<input type="checkbox"/>
Z. Teed and J. Deng: <a href="#">RAFT-3D: Scene Flow using Rigid-Motion Embeddings</a> . arXiv preprint arXiv:2012.00726 2020.									
15	<a href="#">RAFT-it</a>	<a href="#">code</a>	4.11 %	5.34 %	4.31 %	100.00 %	0.1 s	GPU @ 2.5 Ghz (Python)	<input type="checkbox"/>
16	<a href="#">RCA-Flow</a>	<a href="#">code</a>	3.96 %	6.21 %	4.33 %	100.00 %	0.16 s	1 core @ 2.5 Ghz (Python)	<input type="checkbox"/>

(c) KITTI

Figure 13. Screenshot of the supervised fine-tuning results of S-AF on public benchmark. Our method was temporarily named as RAFT-SA+ and RAFT-S-AF.